Physical Communication 80 (2026) 103386

Contents lists available at ScienceDirect

Physical Communication

journal homepage: www.elsevier.com/locate/phycom

Full length article

A unified resource optimization framework for multi-area RIS-UAV communication systems

Xinying Guo [a,*], Longfei Liu [b], Yi Song [a], Jiankang Zhang [c], Sheng Chen [d]

[a] Key Laboratory of Grain Information Processing and Control (Henan University of Technology), Ministry of Education, and College of Information Science and Engineering, Henan University of Technology, Zhengzhou, 450001, China
[b] Mechanical and Electrical Engineering School, Zhengzhou Business University, Gongyi, 451200, China
[c] Department of Computing & Informatics, Bournemouth University, Bournemouth, BH12 5BB, UK
[d] School of Electronics and Computer Science, University of Southampton, Southampton, SO17 1BJ, UK

A R T I C L E I N F O

Keywords:
Beamforming
Multi-area user communication
Reconfigurable intelligent surface
Trajectory optimization
Uncrewed aerial vehicle

A B S T R A C T

We consider a multi-area user (MAU) communication system assisted by an integrated uncrewed aerial vehicle (UAV) and reconfigurable intelligent surface (RIS). In this RIS-UAV assisted MAU communication system, it is essential to collaboratively optimize the base station (BS)'s power allocation and active beamforming, the RIS's passive beamforming, and the RIS-UAV's trajectory to maximize the achievable system weighted sum rate (WSR). To tackle this challenging joint optimization problem, we design a phase-wise alternating convergent algorithm framework that decomposes it into two main phases: the first phase jointly optimizes the BS power allocation, the BS active beamforming and the RIS passive beamforming, while the second phase optimizes the RIS-UAV trajectory. Adopting the same alternating convergent principle to the first phase, we further break down it into two sub-phases, one for optimizing BS power allocation and the other for jointly optimizing the BS active beamforming and the RIS passive beamforming. The two sub-phases are alternately solved by using a convex optimization method and a manifold optimization algorithm based on fractional programming (FP), respectively. For the second phase, a FP-based successive convex approximation (FP-SCA) trajectory optimization algorithm is proposed, which incorporates distance-based user weights to address the issue of communication service fairness among user areas in the MAU system. Simulation results confirm that our distance-based weighted FP-SCA scheme achieves low complexity, significantly enhances the system WSR performance, and ensures the fairness of communication services.

1. Introduction

Uncrewed aerial vehicles (UAVs) have diverse and significant application scenarios in the field of communication, such as restoring emergency communication in disaster areas where communication infrastructure is damaged, alleviating communication congestion in high-traffic areas, and facilitating periodic data distribution or collection in large-scale Internet of Things networks. Also UAVs can offer coverage and connectivity in remote areas where communication infrastructure is lacking, such as mountains and borders, and establish reliable communication links in complex environments where communication links are obstructed, such as in high mountains and cities. Compared to traditional terrestrial communication networks and satellite communication networks, UAV-assisted communication networks possess the advantages of low cost, strong deployability, and high controllability. Consequently, UAV-assisted communication has become one of the indispensable and potential technologies in 6G mobile communication networks [1,2].

The UAV-enabled mobile relay is one of the typical scenarios in UAV-assisted communication. As mobile relays, UAVs offer enhanced flexibility, high cost-effectiveness, and superior mobility in task deployment. Compared to traditional fixed relays, they possess superior potential for optimizing 3D positioning and flight paths, significantly improving communication efficiency. In [3], the authors studied the static UAV and optimized UAV deployment to improve the performance of wireless networks. In [4], the authors extended the static UAV case of [3] to the dynamic UAV case where a UAV flies along fixed trajectory, circling at a constant speed and height. The work [5] studied a scenario where a UAV flies along a circular trajectory at a fixed height, and jointly designed beamforming, circle radius, flight speed and base station (BS)

* Corresponding author.
E-mail addresses: guoxinying@haut.edu.cn (X. Guo), liulf@stu.haut.edu.cn (L. Liu), songyi@haut.edu.cn (Y. Song), jzhang3@bournemouth.ac.uk (J. Zhang), sqc@ecs.soton.ac.uk (S. Chen).

https://doi.org/10.1016/j.phycom.2026.103386
Received 8 August 2026; Received in revised form 6 September 2026; Accepted 17 September 2026
Available online 19 September 2026

power allocation, to maximize energy efficiency (EE). The first study on UAV networks using orthogonal frequency division multiple access technology was conducted in [6].

In practical applications, UAV-enabled mobile relay communication systems encounter a variety of challenges. First, UAVs require substantial energy for flight control and face even higher energy demands during signal transmission and data processing. Their limited on-board energy supply makes flight endurance a primary constraint on their development and application [7]. The study [8] analyzed the various factors affecting UAV energy consumption and established a relationship between energy consumption and relevant parameters. Second, ensuring reliable UAV relay communication in complex wireless environments, such as under adverse weather conditions, is particularly challenging. This affects long-term communication, complex computing tasks, and communication in intricate environments [9]. Notably, these challenges in UAV relay communication systems are expected to be alleviated by the application of reconfigurable intelligent surface (RIS) technology, which can further accelerate the development of 6G networks.

RIS is a technology with programmable electromagnetic properties that dynamically adjusts the amplitude, phase, and polarization of incoming electromagnetic waves to optimize wireless propagation environment and increase transmission efficiency [10–14]. A robust beamforming was designed in [15] for RIS-assisted multi-user equipment (UE) millimeter-wave systems with imperfect channel state information. Research on RIS-assisted secure communications in multi-UE multiple-input multiple-output (MIMO) systems was conducted in [16–18]. The work [19] studied an RIS-aided wireless network, where an RIS with only a finite number of phase shifts at each element is deployed to assist the communication from a multi-antenna access point (AP) to multiple single-antenna users. In [20], a distributed RIS scheme achieved 33% and 68% EE improvements over traditional RIS and amplify-and-forward relay schemes in single-UE and multi-UE scenarios, respectively.

1.1. Related works and motivation

Integrating UAV with RIS leads to RIS-UAV systems. As shown in [21], RIS-UAV systems consume less power and therefore offer higher EE compared with using UAV without RIS. The study [22] investigated the communication quality optimization problem in RIS-UAV systems and validated the feasibility of installing RIS on UAVs for the first time through prototypes. The work [23] studied the maximization of EE in the RIS-UAV based uplink, where the proposed design can increase EE by 38% compared with the traditional UAV scheme without RIS. In [24], a joint RIS passive beamforming and UAV trajectory optimization was addressed, and a successive convex approximation (SCA) scheme was adopted to attain sub-optimal trajectory solutions. The work [25] proposed a security transmission algorithm for RIS-UAV assisted communication networks in the presence of eavesdroppers. Through joint active beamforming and UAV trajectory optimization, the study [26] maximized the spectral efficiency (SE) and EE for RIS-UAV assisted MIMO communication systems. The authors of [27] proposed an active and hybrid RIS-aided UAV relay communication system and demonstrated that the proposed system achieves higher EE than the existing passive RIS and traditional UAV relay systems. Most existing studies on RIS-UAV trajectory optimization focus on single-UE scenarios, neglecting the challenges in multi-UE systems[24–28], resulting in limited applicability of the proposed algorithms.

To further address the aforementioned limitations and explore more advanced optimization strategies in multi-UE environments, recent research has focused on extending RIS-UAV systems to multi-UE scenarios with more complex optimization objectives and constraints. An energy harvesting scheme was proposed in [29] for the RIS-UAV aided multi-UE communication system to enhance the EE of the system. This scheme enables the system to transmit information and harvest energy simultaneously by dividing the passive reflection arrays in geometric space. In order to maximize the weighted sum rate (WSR) of a RIS-UAV assisted multi-UE communication system, the authors of [30] jointly optimized BS active beamforming, RIS passive beamforming and UAV deployment location using the block coordinate descent (BCD) and SCA method. Furthermore, under limited backhaul capacity constraints, the study [31] considered a joint optimization of active/passive beamforming, RIS-UAV trajectory and UE scheduling to maximize the average weighted total rate of the wireless MIMO downlink. By jointly optimizing the passive beamforming and UAV position, the study [32] maximized the system WSR for a RIS-UAV assisted multi-UE cell-free massive MIMO system. It also analyzed the optimal position of RIS-UAV under uniform and non-uniform UE distributions. Notably, existing studies often assume that multi-UE are distributed within a concentrated area [29–33]. This assumption deviates from real-world user deployments in multiple dispersed areas and limits the design of trajectory optimization. Furthermore, the integration of RIS with emerging techniques such as non-orthogonal multiple access (NOMA) and ambient backscatter communications has also attracted considerable attention. For instance, the physical-layer authentication and hardware impairment issues in ambient backscatter-aided NOMA systems were investigated in [34] and [35], respectively, highlighting the importance of secure and reliable RIS-assisted transmissions in resource-constrained scenarios. In this work, we focus on the active-strategy RIS-UAV (ARIS-UAV) paradigm, where the RIS-UAV trajectory is actively optimized, while the passive-strategy RIS-UAV (PRIS-UAV) case with fixed trajectory is used as a performance baseline for comparison.

1.2. Contribution and organization

This paper considers a multi-area user (MAU) communication system assisted by a RIS-UAV, where UEs are distributed across multiple geographically separated user areas (UAs). In order to maximize the system WSR while ensuring service fairness between UAs, we jointly optimize the BS power allocation, active/passive beamforming and RIS-UAV trajectory. Our key contributions are summarized as follows.

1) A RIS-UAV aided MAU system is studied, where UEs are distributed across multiple dispersed UAs. The RIS-UAV flies between predefined starting and ending positions while maintaining service fairness among UAs. In order to maximize the system WSR, a joint optimization framework is developed for BS power allocation, active/passive beamforming and RIS-UAV trajectory. The resulting optimization is non-convex owing to the unit-modulus constraints on beamformings and the coupling of optimization variables.
2) A phase-wise alternating convergent (PAC) algorithm framework is proposed, which decouples this challenging problem into two phases, specifically, the joint optimization phase for the BS power allocation and active/passive beamforming, and the RIS-UAV trajectory optimization phase. We further decompose the BS power allocation and active/passive beamforming joint optimization phase into two sub-phases, namely, the BS power allocation optimization sub-phase and the active/passive beamforming joint optimization sub-phase. For the BS power allocation optimization sub-phase, a convex optimization method is used. For the active/passive beamforming joint optimization sub-phase, a manifold optimization algorithm based on fractional programming (FP) is employed.
3) For the RIS-UAV trajectory optimization phase, the SCA algorithm is widely used due to its ability to convert non-convex problems into convex ones [24,26,28,36]. However, this conversion often leads to a complex objective function and imposes high computational load. To overcome this difficulty, we propose a distance-weighted (DW) FP-SCA algorithm based on the distance information from the UEs to the starting point of the trajectory. This algorithm simplifies the optimization process, reduces complexity, and improves communication fairness in the MAU system by assigning higher weights to users farther from the starting point, thereby enhancing overall network performance.

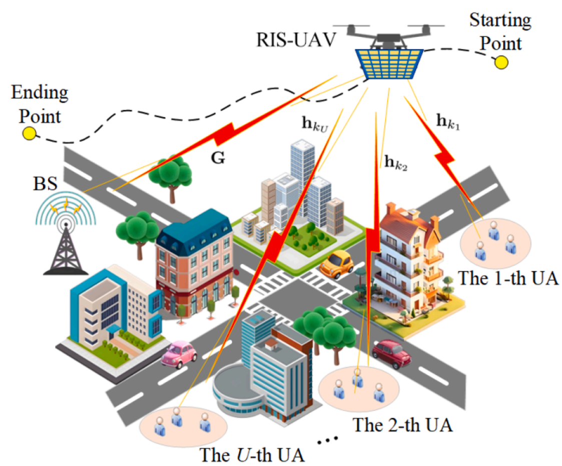

Fig. 1. RIS-UAV aided MAU communication system.

4) Simulations demonstrate that the proposed DW FP-SCA algorithm significantly improves system performance and fairness. Compared with the average weighted (AW) FP-SCA and traditional SCA schemes, our algorithm achieves a higher WSR while ensuring more balanced communication services across all UAs. Specifically, our DW FP-SCA algorithm effectively mitigates the problem of insufficient service time at the far-end UAs by dynamically adjusting the RIS-UAV trajectory and resource allocation based on the designed UE weights. In addition, we conducted simulations to evaluate the convergence time of our proposed algorithm using the traditional SCA algorithm as a benchmark. We also investigated the effects of RIS-UAV deployment altitude, BS transmit power, the number of BS antennas, and the number of RIS units on the achievable system WSR.

The remainder of this paper is structured as follows. The system model and problem formulation are presented in Section 2. Our proposed optimization framework is detailed in Section 3. Complexity analysis of the proposed algorithm is given in Section 4, and the simulation results are provided in Sections 5. Our concluding remarks are offered in Section 6.

Notation: We use italic letters to represent scalars, and lower-case and capital bold-face letters to denote vectors and matrices, respectively. The conjugate, transpose, conjugate transpose and inverse operations are denoted by $[\cdot]^*$, $[\cdot]^{\mathrm{T}}$, $[\cdot]^{\mathrm{H}}$ and $[\cdot]^{-1}$, respectively. $\mathbb{C}^{K\times N}$ represents the $K\times M$-dimensional complex space, $\|\cdot\|$ denotes the Euclidean norm, and $\Re\{\cdot\}$ strands for the real part of a complex-valued number. The circularly symmetric complex Gaussian (CSCG) distribution with zero-mean and variance σ^2 is denoted by $\mathcal{CN}(0,\sigma^2)$. $\mathbf{I}_{K\times K}$ stands for the $K\times K$ identity matrix and the operator $\circ$ signifies element-wise product.

2. System model and problem formulation

2.1. System model

Fig. 1 depicts the RIS-UAV aided MAU communication system conceived. In this system, the BS is assumed to deploys M antennas arranged in a uniform linear array array, while a UAV is integrated with a RIS that has R elements of a uniform planar array. There exist no direct links between the BS and UEs, and signal transmitted by the BS can only be reflected by the RIS to UEs. Each UE is assumed to equip with a single antenna. The RIS-UAV acts as relay to serve U UAs. Let K_u be the number of users in the u-th UA, $u\in\{1,2,\ldots,U\}$, and the number of total users is $K=\sum_{u=1}^{U}K_u$. This clustered distribution imposes unique constraints on the UAV trajectory, as the UAV must serve a group of users within a finite area rather than isolated points. The RIS-UAV commences its journey at the starting point and proceeds to the ending point, navigating along a designated trajectory. Throughout this voyage, it maintains a consistent altitude of H and adheres to a speed of $V_{\max}$. The mission period T is partitioned into N equal-length time slots, and the duration of a time slot is ∇t, i.e., $T=N\nabla t$. Denote the horizontal coordinate of the RIS-UAV in the n-th time slot by $\mathbf{l}_{\mathrm{RIS}}[n]=[x_{\mathrm{RIS}}[n],y_{\mathrm{RIS}}[n]]$, $n\in\mathcal{N}=\{1,2,\ldots,N\}$. Furthermore, the starting point and ending point coordinates of the RIS-UAV are given by $\mathbf{l}_{\mathrm{RIS}}[1]=\mathbf{l}_{\mathrm{I}}$ and $\mathbf{l}_{\mathrm{RIS}}[N]=\mathbf{l}_{\mathrm{F}}$. During the entire flight period, the trajectory of the RIS-UAV satisfies $\|\mathbf{l}_{\mathrm{RIS}}[n+1]-\mathbf{l}_{\mathrm{RIS}}[n]\|^2\le\left(V_{\max}\nabla t\right)^2$, $\forall n$.

The channel linking the BS to the RIS-UAV in the n-th time slot, denoted by $\mathbf{G}[n]\in\mathbb{C}^{R\times M}$, can be expressed as

$$\mathbf{G}[n]=\sqrt{\beta d_{\mathrm{BR}}^{-\kappa}[n]}\mathbf{a}_{\mathrm{RIS}}(\mu[n])\mathbf{a}_{\mathrm{BS}}^{\mathrm{H}}(\psi[n]), \tag{1}$$

in which β denotes the channel power gain at unit distance, κ is the path loss exponent, and $d_{\mathrm{BR}}[n]=\sqrt{H^2+\|\mathbf{l}_{\mathrm{RIS}}[n]-\mathbf{l}_{\mathrm{BS}}\|^2}$ represents the distance from the BS to the RIS-UAV in which $\mathbf{l}_{\mathrm{BS}}=[x_{\mathrm{BS}},y_{\mathrm{BS}}]$ is the horizontal coordinate of the BS. In (1), $\mathbf{a}_{\mathrm{RIS}}(\mu[n])$ is the RIS receive array response vector and $\mathbf{a}_{\mathrm{BS}}(\psi[n])$ is the BS transmit array response vector, where $\mu[n]$ and $\psi[n]$ indicate the RIS-UAV's angle of arrival and the BS's angle of departure information respectively, as elaborated in [37].

Denote the k_u-th UE in the u-th UA by UE_{k_u}, where $k_u\in\mathcal{K}_u=\{1,\ldots,K_u\}$ with $u\in\mathcal{U}=\{1,\ldots,U\}$. Similarly, in the n-th time slot, the channel linking the RIS-UAV to UE_{k_u}, denoted by $\mathbf{h}_{k_u}[n]$, can be expressed as

$$\mathbf{h}_{k_u}[n]=\sqrt{\beta d_{\mathrm{RU},k_u}^{-\tau}[n]}\mathbf{a}_{\mathrm{RIS}}(\omega_{k_u}[n]), \tag{2}$$

where τ is the link's path loss exponent, $d_{\mathrm{RU},k_u}[n]=\sqrt{H^2+\|\mathbf{l}_{\mathrm{RIS}}[n]-\mathbf{l}_{\mathrm{UE},k_u}\|^2}$ is the distance from the RIS-UAV to UE_{k_u}, and $\mathbf{l}_{\mathrm{UE},k_u}=[x_{\mathrm{UE},k_u},y_{\mathrm{UE},k_u}]$ is the horizontal coordinate of UE_{k_u}. The RIS transmit array response vector $\mathbf{a}_{\mathrm{RIS}}(\omega_{k_u}[n])$ in (2) with $\omega_{k_u}[n]$ being the RIS-UAV's angle of departure information to UE_{k_u}, is also referenced in [37].

The complex baseband signal transmitted by the BS in the n-th time slot can be written as

$$\mathbf{x}[n]=\sum_{u=1}^{U}\sum_{k_u=1}^{K_u}\mathbf{w}_{k_u}[n]\sqrt{p_{k_u}[n]}s_{k_u}[n], \tag{3}$$

where $s_{k_u}[n]$ denotes the transmitted data to UE_{k_u}, $p_{k_u}[n]$ represents the power allocated for UE_{k_u}, and $\mathbf{w}_{k_u}[n]\in\mathbb{C}^{M\times 1}$ is the BS's transmit beamforming vector for UE_{k_u}. In the time slot n, we will define $\mathbf{W}[n]=\left[\mathbf{w}_{1_1}[n],\ldots,\mathbf{w}_{K_1}[n],\ldots,\mathbf{w}_{1_U}[n],\ldots,\mathbf{w}_{K_U}[n]\right]^{\mathrm{H}}\in\mathbb{C}^{K\times M}$ as the BS's active beamforming matrix, and $\mathbf{p}[n]=\left[p_{1_1}[n],\ldots,p_{K_1}[n],\ldots,p_{1_U}[n],\ldots,p_{K_U}[n]\right]^{\mathrm{T}}\in\mathbb{C}^{K\times 1}$ as the BS power allocation vector.

2.2. Optimization problem formulation

Our aim is to maximize the achievable system's WSR by jointly optimizing the BS power allocation, active/passive beamforming and RIS-UAV trajectory subject to all the system constraints. To this regard, we first present the signal-to-interference-plus-noise ratio (SINR) of UE_{k_u} in the n-th time slot, denoted by $\gamma_{k_u}[n]$. Define the RIS's phase-shift matrix by $\mathbf{\Phi}[n]=\mathrm{diag}\{\varphi_1[n],\ldots,\varphi_R[n]\}\in\mathbb{C}^{R\times R}$, where $\varphi_r[n]=e^{j\theta_r[n]}$, $\theta_r[n]\in[0,2\pi)$ and $r\in\mathcal{R}=\{1,\ldots,R\}$. Then $\gamma_{k_u}[n]$ is calculated according to

$$\gamma_{k_u}[n]=\frac{\left|\mathbf{h}_{k_u}^{\mathrm{H}}[n]\mathbf{\Phi}[n]\mathbf{G}[n]\mathbf{w}_{k_u}[n]\right|^2p_{k_u}[n]}{\sum\limits_{\tilde{u}=1}^{U}\sum\limits_{\tilde{k}_{\tilde{u}}=1,\tilde{k}_{\tilde{u}}\neq k_u}^{K_{\tilde{u}}}\left|\mathbf{h}_{k_u}^{\mathrm{H}}[n]\mathbf{\Phi}[n]\mathbf{G}[n]\mathbf{w}_{\tilde{k}_{\tilde{u}}}[n]\right|^2p_{\tilde{k}_{\tilde{u}}}[n]+\sigma_\delta^2}, \tag{4}$$

where σ_δ^2 represents the noise power.

Over all the time slots, define the transmission power of the BS as $\mathcal{P}\triangleq\{\mathbf{p}[n],\forall n\}$, the active beamformings at the BS as $\mathcal{W}\triangleq\{\mathbf{W}[n],\forall[n]\}$, the passive beamformings at the RIS as $\mathcal{Z}\triangleq\{\mathbf{\Phi}[n],\forall n\}$, and the trajectory of

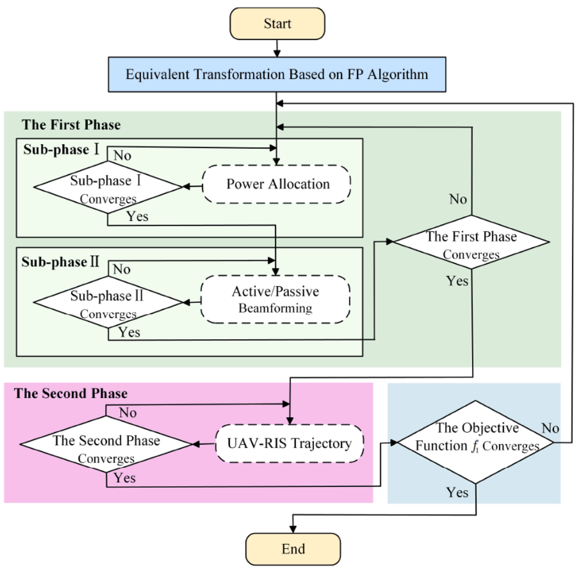

Fig. 2. The PAC algorithm framework.

the RIS-UAV as $\mathcal{Q} \triangleq \{\mathbf{l}_{\mathrm{RIS}}[n], \forall n\}$. Then our proposed WSR maximization problem can be formulated as

$$
\begin{aligned}
\text{(P1)}:\ & \max_{\mathcal{P},\mathcal{W},\mathcal{Z},\mathcal{Q}} f_1(\mathcal{P},\mathcal{W},\mathcal{Z},\mathcal{Q}) \\
& = \frac{1}{N}\sum_{n=1}^{N}\sum_{u=1}^{U}\sum_{k_u=1}^{K_u} \varpi_{k_u} \log_2\left(1+\gamma_{k_u}[n]\right), && \text{(5a)} \\
\text{s.t.}\ & \sum_{u=1}^{U}\sum_{k_u=1}^{K_u} p_{k_u}[n] \le P_{\max}, p_{k_u}[n] > 0, \forall k_u, n, && \text{(5b)} \\
& \|\mathbf{w}_{k_u}[n]\|^2 = 1, \forall k_u, n, && \text{(5c)} \\
& |\varphi_r[n]|^2 = 1, \forall r, n, && \text{(5d)} \\
& \|\mathbf{l}_{\mathrm{RIS}}[n+1] - \mathbf{l}_{\mathrm{RIS}}[n]\|^2 \le (V_{\max}\nabla t)^2, \forall n, && \text{(5e)} \\
& \mathbf{l}_{\mathrm{RIS}}[1] = \mathbf{l}_{\mathrm{I}}, \mathbf{l}_{\mathrm{RIS}}[N] = \mathbf{l}_{\mathrm{F}}, && \text{(5f)}
\end{aligned}
$$

where ϖ_{k_u} is the weight for UE_{k_u}. In this optimization, the constraint (5b) ensures that the BS's total transmission power is within the power limit $P_{\max}$, the constraint (5c) imposes the unit modulus on the BS's active beamforming vectors, and the constraint (5d) ensures the unit modulus for the all RIS's passive beamforming elements, while the constraints (5e) and (5f) ensure the physical feasibility and boundary conditions in the RIS-UAV dynamic adjustment process.

3. Algorithm design for joint optimization

In order to effectively solve the challenging non-convex optimization problem (P1), we design a PAC algorithm framework as shown in Fig. 2. First, the objective function f_1 is converted into a more manageable equivalent form by utilizing the FP technique. Then, the reconstructed problem is decomposed into two optimization phases, with the first phase performing the joint optimization of the BS power allocation and active/passive beamforming, and the second phase carrying out the RIS-UAV trajectory optimization.

The first phase, which involves the joint optimization of BS power allocation and active/passive beamforming, is further divided into the BS power allocation sub-phase and the active/passive beamforming sub-phase, which are iteratively optimized. Each iteration begins with the results from the previous iteration. The process involves optimizing the first sub-phase until convergence, followed by optimizing the second sub-phase until convergence. This sequence continues until the entire first phase converges. The second phase involves the RIS-UAV trajectory optimization, which is addressed using the DW FP-SCA trajectory optimization algorithm proposed in this paper and iterated until convergence.

3.1. Equivalent transformation of optimization (*P*1)

The FP algorithm [38] is utilized to equivalently transform the optimization problem (P1). This equivalent transformation involves applying the Lagrangian dual transformation and the quadratic transformation method.

In order to apply the Lagrangian dual transformation, an auxiliary variable $\chi[n] = \left[\chi_{1_1}[n], \ldots, \chi_{K_1}[n], \ldots, \chi_{1_U}[n], \ldots, \chi_{K_U}[n]\right]^{\mathrm{T}}$ is introduced for the time slot n. By defining $\mathcal{X} \triangleq \{\chi[n], \forall n\}$, the objective function f_1 is equivalent to

$$
\begin{aligned}
f_2(\mathcal{P},\mathcal{W},\mathcal{Z},\mathcal{Q},\mathcal{X}) = \frac{1}{N}\sum_{n=1}^{N}\sum_{u=1}^{U}\sum_{k_u=1}^{K_u} \varpi_{k_u}\Bigg(& \log_2\left(\bar{\chi}_{k_u}[n]\right) \\
& - \chi_{k_u}[n] + \frac{\bar{\chi}_{k_u}[n]|v_{k_u,k_u}[n]|^2 p_{k_u}[n]}{\sum_{\tilde{u}=1}^{U}\sum_{\tilde{k}_{\tilde{u}}=1}^{K_{\tilde{u}}} |v_{k_u,\tilde{k}_{\tilde{u}}}[n]|^2 p_{\tilde{k}_{\tilde{u}}}[n] + \sigma_\delta^2}\Bigg),
\end{aligned}
\tag{6}
$$

where $v_{k_u,\tilde{k}_{\tilde{u}}}[n] = \mathbf{h}_{k_u}^{\mathrm{H}}[n]\mathbf{\Phi}[n]\mathbf{G}[n]\mathbf{w}_{\tilde{k}_{\tilde{u}}}[n]$ and $\bar{\chi}_{k_u}[n] = 1 + \chi_{k_u}[n]$. To apply the quadratic transformation method, an auxiliary variable $\rho[n] = \left[\rho_{1_1}[n], \ldots, \rho_{K_1}[n], \ldots, \rho_{1_U}[n], \ldots, \rho_{K_U}[n]\right]^{\mathrm{T}}$ is introduced for the n-th time slot. By defining $\mathcal{B} \triangleq \{\rho[n], \forall n\}$, the function f_2 can be equivalently transformed into the function f_3 written as (7), shown at the top of next page.

$$
\begin{aligned}
f_3(\mathcal{P},\mathcal{W},\mathcal{Z},\mathcal{Q},\mathcal{X},\mathcal{B}) = \frac{1}{N}\sum_{n=1}^{N}\sum_{u=1}^{U}\sum_{k_u=1}^{K_u} \varpi_{k_u}\Bigg(& \log_2\left(\bar{\chi}_{k_u}[n]\right) - \chi_{k_u}[n] \\
& + 2\sqrt{\bar{\chi}_{k_u}[n] p_{k_u}[n]}\,\Re\left\{\rho_{k_u}^{*}[n] v_{k_u,k_u}[n]\right\} \\
& - |\rho_{k_u}[n]|^2\left(\sum_{\tilde{u}=1}^{U}\sum_{\tilde{k}_{\tilde{u}}=1}^{K_{\tilde{u}}} p_{\tilde{k}_{\tilde{u}}}[n]|v_{k_u,\tilde{k}_{\tilde{u}}}[n]|^2 + \sigma_\delta^2\right)\Bigg).
\end{aligned}
\tag{7}
$$

Then the optimization (P1) is equivalently transformed to the following optimization problem

$$
\begin{aligned}
\text{(P2)}:\ & \max_{\mathcal{P},\mathcal{W},\mathcal{Z},\mathcal{Q},\mathcal{X},\mathcal{B}} f_3(\mathcal{P},\mathcal{W},\mathcal{Z},\mathcal{Q},\mathcal{X},\mathcal{B}), && \text{(8a)} \\
& \text{s.t. (5b), (5c), (5d), (5e), (5f).} && \text{(8b)}
\end{aligned}
$$

When the optimization variables $\mathcal{P}$, $\mathcal{W}$, $\mathcal{Z}$ and $\mathcal{Q}$ are fixed, the optimal $\chi_{k_u}[n]$ and $\rho_{k_u}[n]$, $\forall k_u, n$, are given by

$$
\begin{cases}
\hat{\chi}_{k_u}[n] = \gamma_{k_u}[n], \\
\hat{\rho}_{k_u}[n] = \dfrac{\sqrt{\bar{\chi}_{k_u}[n] p_{k_u}[n]}\, v_{k_u,k_u}[n]}{\sum_{\tilde{u}=1}^{U}\sum_{\tilde{k}_{\tilde{u}}=1}^{K_{\tilde{u}}} p_{\tilde{k}_{\tilde{u}}}[n]|v_{k_u,\tilde{k}_{\tilde{u}}}[n]|^2 + \sigma_\delta^2}.
\end{cases}
\tag{9}
$$

3.2. First phase: BS power allocation and active/passive beamforming joint optimization

Given initial $\mathcal{Q}$, the optimization problem (P2) becomes

$$
\begin{aligned}
\text{(P3)}:\ & \max_{\mathcal{P},\mathcal{W},\mathcal{Z},\mathcal{X},\mathcal{B}} f_3(\mathcal{P},\mathcal{W},\mathcal{Z},\mathcal{X},\mathcal{B}), && \text{(10a)} \\
& \text{s.t. (5b), (5c), (5d).} && \text{(10b)}
\end{aligned}
$$

According to our proposed PAC algorithm framework, the optimization (P3) is further partitioned into two sub-phases.

3.2.1. Sub-phase i BS power allocation optimization

When the optimization variables $\mathcal{W}$ and $\mathcal{Z}$ are given, the optimization problem (P3) becomes

$$
\text{(P4)}:\ \max_{\mathcal{P},\mathcal{X},\mathcal{B}} f_3(\mathcal{P},\mathcal{X},\mathcal{B}), \ \text{s.t. (5b).} \tag{11}
$$

In order to solve (P4), the alternating optimization (AO) algorithm is applied to alternately update the variables $\mathcal{P}$, $\mathcal{X}$ and $\mathcal{B}$ until convergence of $f_3(\mathcal{P},\mathcal{X},\mathcal{B})$ is achieved. More specifically, with $\mathcal{P}$ fixed, $\mathcal{X}$ and $\mathcal{B}$ can be derived according to (9). With given $\mathcal{X}$ and $\mathcal{B}$, the optimization (P4) is a convex problem with respect to $\mathcal{P}$, and this enables us to directly employ the Karush-Kuhn-Tucker conditions to obtain the optimal solution for $p_{k_u}[n]$ as

$$\hat{p}_{k_u}[n]=\left(\frac{\sqrt{\bar{\chi}_{k_u}[n]}\Re\left\{\rho_{k_u}^{*}[n]v_{k_u,k_u}[n]\right\}}{\sum_{\tilde{u}=1}^{U}\sum_{\tilde{k}_{\tilde{u}}=1}^{K_{\tilde{u}}}\left(|\rho_{\tilde{k}_{\tilde{u}}}[n]|^2|v_{k_u,\tilde{k}_{\tilde{u}}}[n]|^2\right)+Lr[n]}\right)^2, \tag{12}$$

where $Lr[n]$ denotes the Lagrange multiplier for the BS's total transmission power constraint (5b), and it can be determined by using the bisection method [39].

3.2.2. Sub-phase II active/passive beamforming joint optimization

Given the optimization variable $\mathcal{P}$, the problem (P3) becomes

$$(\text{P5}): \max_{\mathcal{W},\mathcal{Z},\mathcal{X},\mathcal{B}} f_3(\mathcal{W},\mathcal{Z},\mathcal{X},\mathcal{B}),\ \text{s.t. (5c), (5d)}. \tag{13}$$

Similarly, the AO algorithm can be utilized to solve the problem (P5), which alternately optimizes $\mathcal{W}$, $\mathcal{Z}$, $\mathcal{X}$ and $\mathcal{B}$ until the value $f_3(\mathcal{W},\mathcal{Z},\mathcal{X},\mathcal{B})$ stops improving. Since given $\mathcal{W}$ and $\mathcal{Z}$, the variables $\mathcal{X}$ and $\mathcal{B}$ can be computed according to (9), the key steps in this alternating optimization procedure are the active beamforming optimization and passive beamforming optimization.

2.1) Optimization of Active Beamforming: With given $\mathcal{Z}$, $\mathcal{X}$ and $\mathcal{B}$, the BS's active beamforming matrices $\mathcal{W}$ are optimized. With the aim of facilitating this optimization, the standard Riemannian manifold [40] is adopted to transform the constraint (5c), and the optimization (P5) is reformulated as

$$\max_{\mathcal{W}} f_3(\mathcal{W}),\ \text{s.t. } \mathbf{I}_{K\times K}\circ\left(\mathbf{W}[n]\mathbf{W}^{\mathrm{H}}[n]\right)=\mathbf{I}_{K\times K},\forall n. \tag{14}$$

The Oblique conjugate gradient algorithm [40] is utilized to arrive at the steady-state solution of $f_3(\mathcal{W})$, with the j-th iteration summarized below.

- Compute Oblique gradient:

$$\begin{aligned}\operatorname{grad} f\left(\mathbf{W}^{(j)}[n]\right) &= \nabla f_3\left(\mathbf{W}^{(j)}[n]\right)\\ &-\left(\mathbf{I}_{K\times K}\circ\Re\left\{\mathbf{W}^{(j)}[n](\nabla f_3(\mathbf{W}^{(j)}[n]))^{\mathrm{H}}\right\}\right)\mathbf{W}^{(j)}[n],\end{aligned} \tag{15}$$

where $\nabla f_3(\mathbf{W}^{(j)}[n])$ denotes the standard Euclidean gradient of $f_3(\mathbf{W}^{(j)}[n])$. Denote $\hat{\mathbf{h}}_{k_u}[n]=\mathbf{h}_{k_u}^{\mathrm{H}}[n]\mathbf{\Phi}[n]\mathbf{G}[n]$. Then $\nabla f_3(\mathbf{W}^{(j)}[n])$ is given by (16) at the top of this page.

$$\nabla f_3(\mathbf{W}^{(j)}[n]) = \varpi_{k_u} \times\begin{bmatrix}\sqrt{\bar{\chi}_{1_1}[n]p_{1_1}[n]}\rho_{1_1}^{*}[n]\hat{\mathbf{h}}_{1_1}[n]-\sum_{u=1}^{U}\sum_{k_u=1}^{K_u}|\rho_{k_u}[n]|^2p_{1_1}[n]\mathbf{w}_{1_1}^{\mathrm{H}}[n]\hat{\mathbf{h}}_{k_u}^{\mathrm{H}}[n]\hat{\mathbf{h}}_{k_u}[n]\\ \vdots\\ \sqrt{\bar{\chi}_{K_1}[n]p_{K_1}[n]}\rho_{K_1}^{*}[n]\hat{\mathbf{h}}_{K_1}[n]-\sum_{u=1}^{U}\sum_{k_u=1}^{K_u}|\rho_{k_u}[n]|^2p_{K_1}[n]\mathbf{w}_{K_1}^{\mathrm{H}}[n]\hat{\mathbf{h}}_{k_u}^{\mathrm{H}}[n]\hat{\mathbf{h}}_{k_u}[n]\\ \vdots\\ \sqrt{\bar{\chi}_{1_U}[n]p_{1_U}[n]}\rho_{1_U}^{*}[n]\hat{\mathbf{h}}_{1_U}[n]-\sum_{u=1}^{U}\sum_{k_u=1}^{K_U}|\rho_{k_u}[n]|^2p_{1_U}[n]\mathbf{w}_{1_U}^{\mathrm{H}}[n]\hat{\mathbf{h}}_{k_u}^{\mathrm{H}}[n]\hat{\mathbf{h}}_{k_u}[n]\\ \vdots\\ \sqrt{\bar{\chi}_{K_U}[n]p_{K_U}[n]}\rho_{K_U}^{*}[n]\hat{\mathbf{h}}_{K_U}[n]-\sum_{u=1}^{U}\sum_{k_u=1}^{K_U}|\rho_{k_u}[n]|^2p_{K_U}[n]\mathbf{w}_{K_U}^{\mathrm{H}}[n]\hat{\mathbf{h}}_{k_u}^{\mathrm{H}}[n]\hat{\mathbf{h}}_{k_u}[n]\end{bmatrix}. \tag{16}$$

- Determine the search direction:

$$\mathbf{D}_{\mathrm{W}}^{(j)}[n]=-\operatorname{grad} f\left(\mathbf{W}^{(j)}[n]\right)+\beta_{\mathrm{W}}^{(j)}[n]\mathcal{T}_{\mathrm{W}}\left(\mathbf{D}_{\mathrm{W}}^{(j-1)}[n]\right), \tag{17}$$

where $\beta_{\mathrm{W}}^{(j)}[n]$ is the Polak-Ribiére conjugate gradient update parameter given by

$$\beta_{\mathrm{W}}^{(j)}[n]=\frac{\nabla f_3^{\mathrm{H}}(\mathbf{W}^{(j)}[n])\left(\nabla f_3(\mathbf{W}^{(j)}[n])-\mathcal{T}_{\mathrm{W}}(\nabla f_3(\mathbf{W}^{(j-1)}[n]))\right)}{\|\nabla f_3(\mathbf{W}^{(j-1)}[n])\|^2}, \tag{18}$$

and $\mathcal{T}_{\mathrm{W}}(\mathbf{D}_{\mathrm{W}}^{(j-1)}[n])$ is the projection function, which is expressed by

$$\begin{aligned}\mathcal{T}_{\mathrm{W}}\left(\mathbf{D}_{\mathrm{W}}^{(j-1)}[n]\right)&=\mathbf{D}_{\mathrm{W}}^{(j-1)}[n]\\ &-\left(\mathbf{I}_{K\times K}\circ\Re\left\{\mathbf{W}^{(j)}[n](\mathbf{D}_{\mathrm{W}}^{(j-1)}[n])^{\mathrm{H}}\right\}\right)\mathbf{W}^{(j)}[n].\end{aligned} \tag{19}$$

- Retract back onto Oblique manifold and update:

Apply the Armijo backtracking line search algorithm to determine the step size $u_1[n]$, retract back onto Oblique manifold and update $\mathbf{W}^{(j+1)}[n]$ as given by (20) at the bottom of this page, where $w_{im}[n]$ and $d_{\mathrm{W},im}^{(j)}[n]$ denotes the i-th row and m-th column elements of $\mathbf{W}[n]$ and $\mathbf{D}_{\mathrm{W}}^{(j)}[n]$, respectively.

$$\mathbf{W}^{(j+1)}[n] = \begin{bmatrix}\frac{w_{1_1 1}^{(j)}[n]+u_1[n]d_{\mathrm{W},1_1 1}^{(j)}[n]}{\sqrt{\sum_{u=1}^{U}\sum_{k_u=1}^{K_u}|w_{k_u 1}^{(j)}[n]+u_1[n]d_{\mathrm{W},k_u 1}^{(j)}[n]|^2}} & \cdots & \frac{w_{1_1 M}^{(j)}[n]+u_1[n]d_{\mathrm{W},1_1 M}^{(j)}[n]}{\sqrt{\sum_{u=1}^{U}\sum_{k_u=1}^{K_u}|w_{k_u M}^{(j)}[n]+u_1[n]d_{\mathrm{W},k_u M}^{(j)}[n]|^2}}\\ & \vdots & \\ \frac{w_{K_1 1}^{(j)}[n]+u_1[n]d_{\mathrm{W},K_1 1}^{(j)}[n]}{\sqrt{\sum_{u=1}^{U}\sum_{k_u=1}^{K_u}|w_{k_u 1}^{(j)}[n]+u_1[n]d_{\mathrm{W},k_u 1}^{(j)}[n]|^2}} & \cdots & \frac{w_{K_1 M}^{(j)}[n]+u_1[n]d_{\mathrm{W},K_1 M}^{(j)}[n]}{\sqrt{\sum_{u=1}^{U}\sum_{k_u=1}^{K_u}|w_{k_u M}^{(j)}[n]+u_1[n]d_{\mathrm{W},k_u M}^{(j)}[n]|^2}}\\ & \vdots & \\ \frac{w_{1_U 1}^{(j)}[n]+u_1[n]d_{\mathrm{W},1_U 1}^{(j)}[n]}{\sqrt{\sum_{u=1}^{U}\sum_{k_u=1}^{K_u}|w_{k_u 1}^{(j)}[n]+u_1[n]d_{\mathrm{W},k_u 1}^{(j)}[n]|^2}} & \cdots & \frac{w_{1_U M}^{(j)}[n]+u_1[n]d_{\mathrm{W},1_U M}^{(j)}[n]}{\sqrt{\sum_{u=1}^{U}\sum_{k_u=1}^{K_u}|w_{k_u M}^{(j)}[n]+u_1[n]d_{\mathrm{W},k_u M}^{(j)}[n]|^2}}\\ & \vdots & \\ \frac{w_{K_U 1}^{(j)}[n]+u_1[n]d_{\mathrm{W},K_U 1}^{(j)}[n]}{\sqrt{\sum_{u=1}^{U}\sum_{k_u=1}^{K_u}|w_{k_u 1}^{(j)}[n]+u_1[n]d_{\mathrm{W},k_u 1}^{(j)}[n]|^2}} & \cdots & \frac{w_{K_U M}^{(j)}[n]+u_1[n]d_{\mathrm{W},K_U M}^{(j)}[n]}{\sqrt{\sum_{u=1}^{U}\sum_{k_u=1}^{K_u}|w_{k_u M}^{(j)}[n]+u_1[n]d_{\mathrm{W},k_u M}^{(j)}[n]|^2}}\end{bmatrix}, \tag{20}$$

2.2) Optimization of Passive Beamforming: Given the optimization variables $\mathcal{W}$, $\mathcal{X}$ and $\mathcal{B}$, the passive beamforming diagonal matrices $\mathcal{Z}$ are optimized. By defining $\mathbf{h}_{k_u}^{\mathrm{H}}[n]\mathbf{\Phi}[n]\mathbf{G}[n]\mathbf{w}_i[n]=\boldsymbol{\varphi}^{\mathrm{H}}[n]\mathrm{diag}\left\{\mathbf{h}_{k_u}^{\mathrm{H}}[n]\right\}\mathbf{G}[n]\mathbf{w}_i[n]=\boldsymbol{\varphi}^{\mathrm{H}}[n]\mathbf{z}_{k_u,i}[n]$, where $\boldsymbol{\varphi}[n]=\left[\varphi_1[n],\ldots,\varphi_R[n]\right]^{\mathrm{H}}$, the problem (P5) can be rewritten as

$$\begin{aligned}\min_{\boldsymbol{\varphi}[n]} \frac{1}{N}\sum_{n=1}^{N}\sum_{u=1}^{U}\sum_{k_u=1}^{K_u} f_4(\boldsymbol{\varphi}[n]) = \varpi_{k_u}\Big(&\boldsymbol{\varphi}^{\mathrm{H}}[n]\mathbf{A}[n]\boldsymbol{\varphi}[n]\\ &-2\sqrt{\bar{\chi}_{k_u}[n]p_{k_u}[n]}\Re\left\{\boldsymbol{\varphi}^{\mathrm{H}}[n]\mathbf{b}[n]\right\}\Big),\end{aligned} \tag{21a}$$

$$\text{s.t. (5d)}, \tag{21b}$$

where $\mathbf{A}[n]=\left(|\rho_{k_u}[n]|^2\sum_{\tilde{u}=1}^{U}\sum_{\tilde{k}=1}^{K_{\tilde{u}}}\mathbf{z}_{k_u,\tilde{k}_{\tilde{u}}}[n]\mathbf{z}_{k_u,\tilde{k}_{\tilde{u}}}^{\mathrm{H}}[n]p_{\tilde{k}_{\tilde{u}}}[n]\right)\in\mathbb{C}^{R\times R}$ and $\mathbf{b}[n]=\rho_{k_u}^{*}[n]\mathbf{z}_{k_u,k_u}[n]\in\mathbb{C}^{R\times 1}$. We employ the Riemannian conjugate gradient algorithm to arrive at the steady-state solution of $f_4(\boldsymbol{\varphi}[n])$ [41], with the j-th iteration detailed below.

- Calculation of Oblique gradient:

$$\begin{aligned}\operatorname{grad} f(\boldsymbol{\varphi}^{(j)}[n])&=\nabla f_4(\boldsymbol{\varphi}^{(j)}[n])\\ &-\Re\{\nabla f_4(\boldsymbol{\varphi}^{(j)}[n])\circ(\boldsymbol{\varphi}^{(j)}[n])^{*}\}\circ\boldsymbol{\varphi}^{(j)}[n],\end{aligned} \tag{22}$$

where $\nabla f_4(\boldsymbol{\varphi}^{(j)}[n])$ denotes the Euclidean gradient of $f_4(\boldsymbol{\varphi}^{(j)}[n])$, expressed as

$$\nabla f_4(\boldsymbol{\varphi}^{(j)}[n]) = \varpi_{k_u}\left(\mathbf{A}[n]\boldsymbol{\varphi}^{(j)}[n]-\Re\{\mathbf{b}[n]\}\right). \tag{23}$$

- Determine the search direction:

$$\mathbf{d}_{\Phi}^{(j)}[n]=-\operatorname{grad} f(\boldsymbol{\varphi}^{(j)}[n])+\beta_{\Phi}^{(j)}[n]\mathcal{T}_{\Phi}\left(\mathbf{d}_{\Phi}^{(j-1)}[n]\right), \tag{24}$$

where $\beta_{\Phi}^{(j)}[n]$ is similar to $\beta_{\mathrm{W}}^{(j)}[n]$ in (16), and $\mathcal{T}_{\Phi}\left(\mathbf{d}_{\Phi}^{(j-1)}[n]\right)$ denotes the projection function

$$\begin{aligned}\mathcal{T}_{\Phi}\left(\mathbf{d}_{\Phi}^{(j-1)}[n]\right)&=\mathbf{d}_{\Phi}^{(j-1)}[n]\\ &-\Re\left\{\mathbf{d}_{\Phi}^{(j-1)}[n]\circ(\boldsymbol{\varphi}^{(j)}[n])^{*}\right\}\circ\boldsymbol{\varphi}^{(j)}[n].\end{aligned} \tag{25}$$

- Retract back onto Riemannian manifold and update:

Apply the Armijo backtracking line search algorithm to select the step size $u_2[n]$, retract back onto Riemannian manifold, and update $\boldsymbol{\varphi}^{(j+1)}[n]$:

$$\boldsymbol{\varphi}^{(j+1)}[n]=\left[\frac{\varphi_1[n]+u_2[n]d_{\Phi,1}^{(j)}[n]}{|\varphi_1[n]+u_2[n]d_{\Phi,1}^{(j)}[n]|},\ldots,\frac{\varphi_R[n]+u_2[n]d_{\Phi,R}^{(j)}[n]}{|\varphi_R[n]+u_2[n]d_{\Phi,R}^{(j)}[n]|}\right]^{\mathrm{T}}. \tag{26}$$

3.3. Second phase: RIS-UAV trajectory optimization

In this phase, given $\mathcal{P}$, $\mathcal{W}$ and $\mathcal{Z}$, the problem (P2) is reformulated as

$$\text{(P6)}: \max_{\mathcal{Q},\mathcal{X},\mathcal{B}} f_3(\mathcal{Q},\mathcal{X},\mathcal{B}), \tag{27a}$$

$$\text{s.t. (5e), (5f).} \tag{27b}$$

where $\mathcal{X}$ and $\mathcal{B}$ can be updated by (9). The channel linking the BS and the RIS-UAV as well as the channel linking the RIS-UAV to UE_{k_u} are rephrased respectively as

$$\mathbf{G}[n] = \frac{\hat{\mathbf{G}}[n]}{d_{\text{BR}}^{\frac{\kappa}{2}}[n]},\ \mathbf{h}_{k_u}[n] = \frac{\hat{\mathbf{h}}_{k_u}[n]}{d_{\text{RU},k_u}^{\frac{\tau}{2}}[n]}, \tag{28}$$

where

$$\hat{\mathbf{G}}[n] = \sqrt{\beta}\mathbf{a}_{\text{RIS}}(\mu[n])\mathbf{a}_{\text{BS}}^{\text{H}}(\psi[n]), \tag{29}$$

$$\hat{\mathbf{h}}_{k_u}[n] = \sqrt{\beta}\mathbf{a}_{\text{RIS}}(\omega_{k_u}[n]). \tag{30}$$

Then the RIS-UAV trajectory optimization problem (P6) is reformulated as

$$\text{(P7)}: \max_{\mathcal{Q}} \frac{1}{N}\sum_{n=1}^{N}\sum_{u=1}^{U}\sum_{k_u=1}^{K_u}\varpi_{k_u}\left(\frac{E_{k_u}^{(1)}[n]}{d_{\text{RU},k_u}^{\frac{\tau}{2}}[n]d_{\text{BR}}^{\frac{\kappa}{2}}[n]} - \frac{E_{k_u}^{(2)}[n]}{d_{\text{RU},k_u}^{\tau}[n]d_{\text{BR}}^{\kappa}[n]}\right), \tag{31a}$$

$$\text{s.t. (5e), (5f),} \tag{31b}$$

where

$$E_{k_u}^{(1)}[n]{=}2\sqrt{\bar{\chi}_{k_u}[n]p_{k_u}[n]}\Re\{\rho_{k_u}^{*}[n]\hat{\mathbf{h}}_{k_u}^{\text{H}}[n]\mathbf{\Phi}[n]\hat{\mathbf{G}}[n]\mathbf{w}_{k_u}[n]\}, \tag{32}$$

$$E_{k_u}^{(2)}[n]{=}|\rho_{k_u}[n]|^2\sum_{\tilde{u}=1}^{U}\sum_{\bar{k}_{\tilde{u}}=1}^{K_{\tilde{u}}}p_{\bar{k}_{\tilde{u}}}[n]|\hat{\mathbf{h}}_{k_u}^{\text{H}}[n]\mathbf{\Phi}[n]\hat{\mathbf{G}}[n]\mathbf{w}_{\bar{k}_{\tilde{u}}}[n]|^2. \tag{33}$$

Since the objective function (31a) is nonlinear with respect to $\mathcal{Q}$, (P7) is a non-convex optimization problem. By introducing relaxation variables $x_{\text{RU},k_u}[n]$ and $x_{\text{BR}}[n]$ to relax $d_{\text{RU},k_u}[n]$ and $d_{\text{BR}}[n]$ [28], the optimization problem (P7) can be reformulated as

$$\text{(P8)}: \max_{\mathcal{Q},\mathcal{X}_{\text{RU}},\mathcal{X}_{\text{BR}}} \frac{1}{N}\sum_{n=1}^{N}\sum_{u=1}^{U}\sum_{k_u=1}^{K_u}\varpi_{k_u}\left(\frac{E_{k_u}^{(1)}[n]}{x_{\text{RU},k_u}^{\frac{\tau}{2}}[n]x_{\text{BR}}^{\frac{\kappa}{2}}[n]} - \frac{E_{k_u}^{(2)}[n]}{x_{\text{RU},k_u}^{\tau}[n]x_{\text{BR}}^{\kappa}[n]}\right), \tag{34a}$$

$$\text{s.t. } x_{\text{RU},k_u}[n] \geq d_{\text{RU},k_u}[n],\ \forall k_u, n, \tag{34b}$$

$$x_{\text{BR}}[n] \geq d_{\text{BR}}[n],\ \forall n, \tag{34c}$$

$$\text{(5e), (5f),} \tag{34d}$$

where $\mathcal{X}_{\text{RU}} \triangleq \{x_{\text{RU},k_u}[n], \forall k_u, n\}$ and $\mathcal{X}_{\text{BR}} \triangleq \{x_{\text{BR}}[n], \forall n\}$. Using the SCA algorithm, the first-order Taylor expansions of (34b) and (34c) at points $x_{\text{RU},k_u,0}[n]$ and $x_{\text{BR},0}[n]$ are given respectively as

$$x_{\text{RU},k_u}^2[n] \geq 2x_{\text{RU},k_u}[n]x_{\text{RU},k_u,0}[n] - x_{\text{RU},k_u,0}^2[n], \tag{35}$$

$$x_{\text{BR}}^2[n] \geq 2x_{\text{BR}}[n]x_{\text{BR},0}[n] - x_{\text{BR},0}^2[n]. \tag{36}$$

The objective function (34a) has the first-order Taylor expansion at points $x_{\text{RU},k_u,0}[n]$ and $x_{\text{BR},0}[n]$, given in (37) at the top of next page, where

$$f_5(\mathcal{Q},\mathcal{X}_{\text{RU}},\mathcal{X}_{\text{BR}}) \geq \frac{1}{N}\sum_{n=1}^{N}\sum_{u=1}^{U}\sum_{k_u=1}^{K_u}\varpi_{k_u}\big(Z_{k_u,0}^{(1)}[n] + Z_{k_u,0}^{(2)}[n](x_{\text{RU},k_u}[n] - x_{\text{RU},k_u,0}[n]) + Z_{k_u,0}^{(3)}[n](x_{\text{BR}}[n] - x_{\text{BR},0}[n])\big), \tag{37}$$

$$Z_{k_u,0}^{(1)}[n] = \frac{E_{k_u}^{(1)}[n]}{x_{\text{RU},k_u,0}^{\frac{\tau}{2}}[n]x_{\text{BR},0}^{\frac{\kappa}{2}}[n]} - \frac{E_{k_u}^{(2)}[n]}{x_{\text{RU},k_u,0}^{\tau}[n]x_{\text{BR},0}^{\kappa}[n]}, \tag{38}$$

$$Z_{k_u,0}^{(2)}[n] = \frac{\partial Z_{k_u,0}^{(1)}[n]}{\partial x_{\text{RU},k_u,0}[n]} = -\frac{\tau}{2}x_{\text{RU},k_u,0}^{-\frac{\tau}{2}-1}[n]x_{\text{BR},0}^{-\frac{\kappa}{2}}[n]E_{k_u}^{(1)}[n] + \tau x_{\text{RU},k_u,0}^{-\tau-1}[n]x_{\text{BR},0}^{-\kappa}[n]E_{k_u}^{(2)}[n], \tag{39}$$

$$Z_{k_u,0}^{(3)}[n] = \frac{\partial Z_{k_u,0}^{(1)}[n]}{\partial x_{\text{BR},0}[n]} = -\frac{\kappa}{2}x_{\text{BR},0}^{-\frac{\kappa}{2}-1}[n]x_{\text{RU},k_u,0}^{-\frac{\tau}{2}}[n]E_{k_u}^{(1)}[n] + \kappa x_{\text{BR},0}^{-\kappa-1}[n]x_{\text{RU},k_u,0}^{-\tau}[n]E_{k_u}^{(2)}[n]. \tag{40}$$

According to (35) – (37), (P8) can be rewritten by

$$\text{(P9)}: \max_{\mathcal{Q},\mathcal{X}_{\text{RU}},\mathcal{X}_{\text{BR}}} \frac{1}{N}\sum_{n=1}^{N}\sum_{u=1}^{U}\sum_{k_u=1}^{K_u}\varpi_{k_u}\Big(Z_{k_u,0}^{(2)}[n]x_{\text{RU},k_u}[n] + Z_{k_u,0}^{(3)}[n]x_{\text{BR}}[n]\Big), \tag{41a}$$

$$\text{s.t. (35), (36), (5e), (5f).} \tag{41b}$$

The convex optimization problem (P9) can readily be solved using the CVX [28].

In addition to BS power allocation, active/passive beamforming and trajectory optimization, user weights ϖ_{k_u} are also important for system WSR performance. In the MAU communication system, adopting the average weight for ϖ_{k_u} tends to allocate more service time slots of the RIS-UAV to the UA closer to the starting point. This average-weighted (AW) design strategy results in service unfairness. The root cause of this issue lies in the distance-dependent nature of the system optimization process and the coupling between variables.

As illustrated in Fig. 3, consider a scenario with three UAs in the MAU system. The initial trajectory involves the RIS-UAV flying in a straight line from the starting point to the ending point, and the entire flight duration is divided into 30 equal-length time slots. Based on the positional relationship between the UAs and the trajectory, it is assumed that the first 10 time slots serve the 1st UA, the middle 10 time slots serve the 2nd UA, and the last 10 time slots serve the 3rd UA. In the first phase, the system allocates power and beamforming resources to the UA that is closer to the RIS-UAV. To ensure user fairness, an average weight design should be adopted. However, in the second phase[1], the RIS-UAV adjusts its trajectory to be closer to the 1st UA during the first 10 time slots in order to maximize the WSR. This adjustment is driven by the fact that closer distances result in better channel conditions. As a consequence, some of the time slots serving UAs farther from the starting point will be transferred to UAs closer to the starting point. As the iterations proceed, more and more time slots will be allocated to serve the 1st UA.

To address the service unfairness caused by the geographical separation of UAs in the MAU system, we propose a distance-based weight design method. Unlike traditional multi-user systems, where fairness is typically managed through proportional fairness, the large inter-area distance disparity in MAU systems necessitates a mechanism to compensate for the severe path loss experienced by far-end areas. In the proposed method, the weights for users in far-end areas are increased according to a power function of their distance. The expression for the distance-based weight ϖ_{k_u} of UE_{k_u} is as follows

$$\varpi_{k_u} = \frac{(d_{\text{RU},k_u}[1])^{\tau}}{\sum_{u=1}^{U}\sum_{k_u=1}^{K_u}(d_{\text{RU},k_u}[1])^{\tau}}. \tag{42}$$

where $d_{\text{RU},k_u}[1]$ is the starting point distance between UE_{k_u} and the starting point.

Within the PAC framework, the first and second phases are executed alternately and iteratively until overall convergence. Specifically, once

[1] We only consider the time slots serving the UAs, and do not depict the specific flight trajectory.

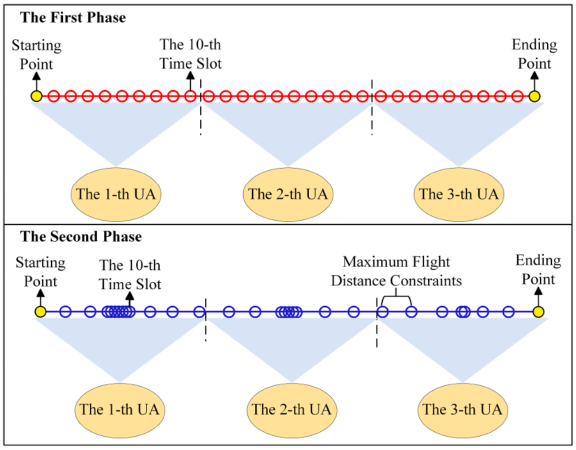

Fig. 3. Schematic representation of unfairness in time-slot services.

Algorithm 1 Proposed PAC algorithm framework for joint optimization.

Initialize $\mathcal{P}^{(0)}, \mathcal{W}^{(0)}, \mathcal{Z}^{(0)}$ and $\mathcal{Q}^{(0)}$, Set $t_1 = t_2 = 0$;
The first phase:
repeat
  $t_1 = t_1 + 1$, $t_{1,1} = t_{1,2} = 0$;
  repeat
    $t_{1,1} = t_{1,1} + 1$;
    Update variables $\mathcal{X}^{(t_{1,1})}$ and $\mathcal{B}^{(t_{1,1})}$ by (9);
    Update BS power allocation vector $\mathcal{P}^{(t_{1,1})}$ by (12);
  until (P4) converges.
  repeat
    $t_{1,2} = t_{1,2} + 1$;
    Update variables $\mathcal{X}^{(t_{1,2})}$ and $\mathcal{B}^{(t_{1,2})}$ by (9);
    Update active beamforming $\mathcal{W}^{(t_{1,2})}$ by (20);
    Update variables $\tilde{\boldsymbol{\varphi}}^{(t_{1,2})}$ by (26);
    Update passive beamforming $\mathcal{Z}^{(t_{1,2})} = \text{diag}\{\tilde{\boldsymbol{\varphi}}^{(t_{1,2})}\}$;
  until (P5) converges.
  $\mathcal{P}^{(t_1)} = \mathcal{P}^{(t_{1,1})}$, $\mathcal{Z}^{(t_1)} = \mathcal{Z}^{(t_{1,2})}$, $\mathcal{W}^{(t_1)} = \mathcal{W}^{(t_{1,2})}$;
until (P3) converges.
The second phase:
repeat
  $t_2 = t_2 + 1$;
  Update variables $\mathcal{X}^{(t_2)}$ and $\mathcal{B}^{(t_2)}$ by (9);
  Update $\mathcal{Q}^{(t_2)}$ by solving (P9);
until (P6) converges.
Repeat the first phase.
Output optimal $\mathcal{P}^{(t_1)}$, $\mathcal{Z}^{(t_1)}$, $\mathcal{W}^{(t_1)}$ and $\mathcal{Q}^{(t_2)}$.

the second phase converges, the first phase is re-executed using the updated UAV-RIS trajectory to refine beamforming and power allocation.

4. Algorithm analysis

Algorithm 1 summarizes the proposed PAC algorithm framework for joint optimization of $\mathcal{P}, \mathcal{W}, \mathcal{Z}$ and $\mathcal{Q}$. The computational complexity of the proposed algorithm primarily arises from solving the optimization problems for BS power allocation, active/passive beamforming, and RIS-UAV trajectory optimization. Specifically, the BS power allocation optimization algorithm and the joint active/passive beamforming optimization algorithm impose the computational complexity on the orders of $\mathcal{O}(I_1 K^3)$ and $\mathcal{O}(I_2(MK^2 + RK^2))$, respectively, where I_1 and I_2 are the numbers of iterations in the first and second sub-phases, respectively. Consequently, the computational complexity of the first phase is on the order of $\mathcal{O}(I_{O,1}(I_1 K^3 + I_2(MK^2 + RK^2)))$, where $I_{O,1}$ denotes the number of iterations associated with the first phase.

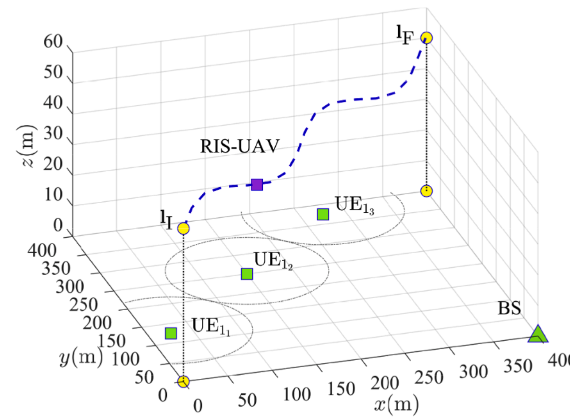

Fig. 4. The 3D coordinate system configuration.

Furthermore, the RIS-UAV trajectory optimization is solved using the SCA algorithm in combination with the CVX toolbox. The complexity of this optimization depends on the number of variables, the structure of the objective function, and the optimization constraints. The CVX toolbox, which typically employs the interior-point method to solve convex optimization problems, has the computational complexity proportional to the 3.5-th power of the number of variables [42]. For the traditional SCA trajectory optimization algorithm [28,43], the complexity of computing the objective function is on the order of $\mathcal{O}(K^2(RM)^2)$, and the overall complexity is $\mathcal{O}(I_{O,2}((NK)^{3.5} + K^2(RM)^2))$, where $I_{O,2}$ represents the number of iterations in the second phase. In contrast, our DW FP-SCA trajectory optimization algorithm simplifies the objective function, reducing its complexity to $\mathcal{O}(K(K+1)RM)$. As a result, the total complexity of the DW FP-SCA algorithm is $\mathcal{O}(I_{O,2}((NK)^{3.5} + K(K+1)RM))$. Compared to the traditional SCA algorithm, our DW FP-SCA algorithm significantly reduces computational complexity by optimizing the expression of the objective function. It eliminates high-order terms and nested operations in the objective function and reduces the computational burden during the solving process while maintaining algorithmic performance.

5. Simulations

In our simulations, the RIS-UAV is configured as ARIS-UAV, meaning that its trajectory is dynamically optimized as part of the joint resource allocation framework. For comparison, we also include PRIS-UAV baseline, where the RIS-UAV follows a fixed straight-line trajectory or a non-optimized path, to highlight the performance gains achieved by trajectory optimization.

A RIS-UAV assisted MAU system with $U = 3$ UAs is simulated. To validate the effectiveness of the proposed algorithms, we assume full knowledge of the channel state information. The channel power gain per unit distance is chosen to be $\beta = -30$ dB, the path loss exponents for the channel from the BS to the RIS-UAV and the channel from the RIS-UAV to each UE are set to $\kappa = \tau = 2$, and the noise power spectral density is set to -174 dBm/Hz. Unless otherwise specified, the following default system's parameters are used: the number of BS antennas is $M = 30$, the number of RIS units is $R = 100$, the number of UEs in each UA is $K_u = 1$, $u = 1, 2, 3$, i.e., $K = 3$, the maximum BS transmitting power is set to $P_{\max} = 30$ dBm. Fig. 4 illustrates the system geographical configuration, where the BS horizontal coordinate is $\mathbf{l}_{\mathrm{BS}} = [400, 0]$ m, and the three UE horizontal coordinates are $\mathbf{l}_{\mathrm{UE},1} = [25, 125]$ m, $\mathbf{l}_{\mathrm{UE},2} = [150, 250]$ m and $\mathbf{l}_{\mathrm{UE},3} = [275, 375]$ m, respectively. The RIS-UAV flies from the starting point $\mathbf{l}_\mathrm{I} = [0, 0]$ m to the ending point $\mathbf{l}_\mathrm{F} = [400, 400]$ m, with the height $H = 40$ m and the maximum speed $V_{\max} = 25$ m/s. The flight period is divided into 30 equal-length time slots, each with a duration of $\nabla t = 2$ s. Note that perfect CSI is assumed here to establish a theoretical performance upper bound. In practical scenarios, the CSI acquisition errors,

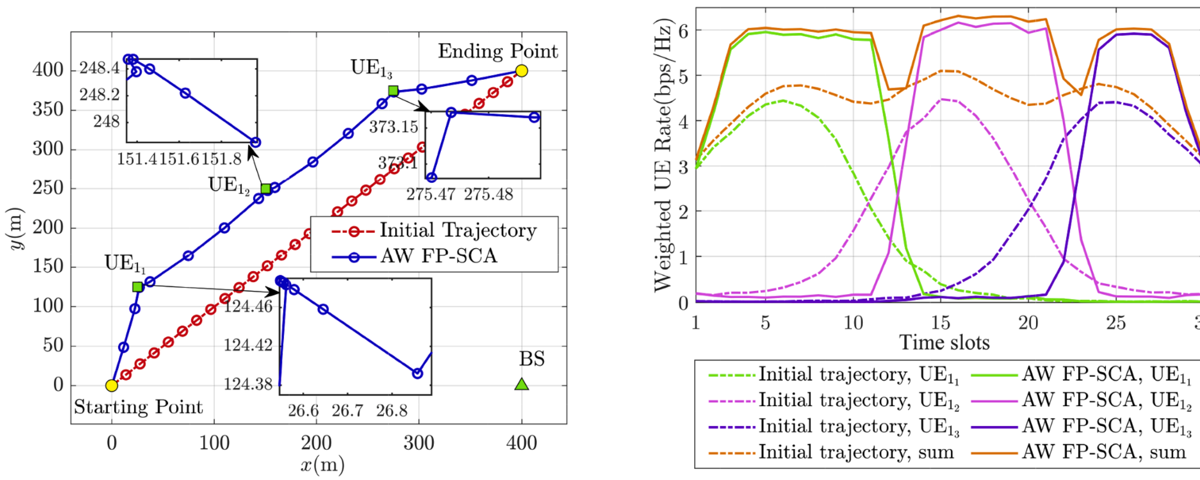

(a) (b)

Fig. 5. (a) RIS-UAV flight trajectory with the AW FP-SCA algorithm, (b) Weighted UE rate under different time slots with the AW FP-SCA algorithm.

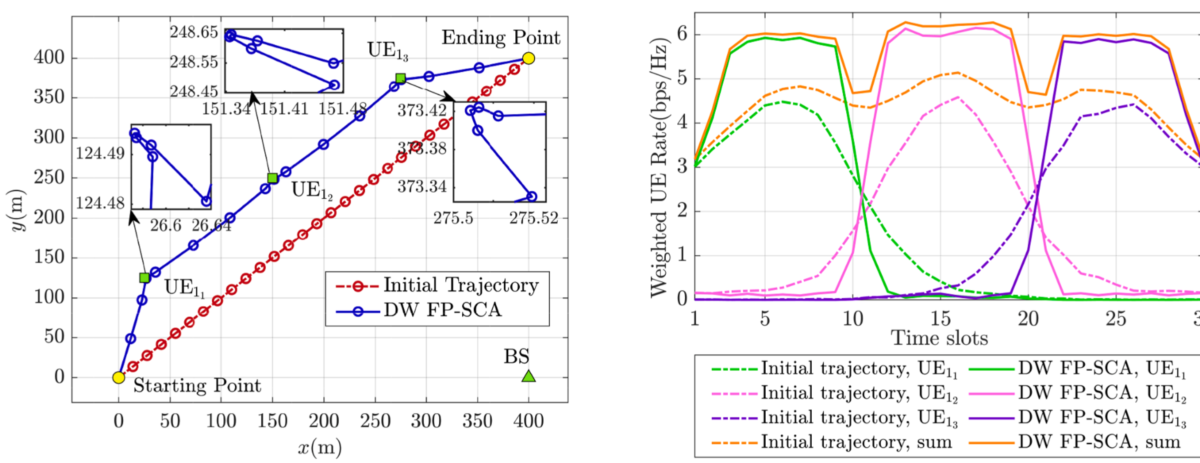

(a) (b)

Fig. 6. (a) RIS-UAV flight trajectory with the proposed DW FP-SCA algorithm, (b) Weighted UE rate under different time slots with the proposed DW FP-SCA algorithm.

overhead and blockage issues faced by practical RIS systems are also directions worthy of further investigation [44,45].

To demonstrate the unfairness of the commonly used AW strategy, we first investigate the AW FP-SCA trajectory optimization scheme. Fig. 5(a) depicts the flight trajectory of the RIS-UAV under the initial trajectory scheme and the AW FP-SCA trajectory optimization scheme. It is evident that with the AW FP-SCA algorithm, the RIS-UAV allocates more time slots to hover above UE_{1_1} and only three time slots to hover above UE_{1_3}, as illustrated in Fig. 3. Fig. 5(b) demonstrates the weighted UE rate and the corresponding sum rate under different time slots for both the initial trajectory scheme and the AW FP-SCA trajectory optimization scheme, respectively. As expected, the AW FP-SCA algorithm improves the weighted UE rate at each time slot compared to the initial trajectory scheme. Furthermore, by comparing the weighted UE rate per time slot for UE_{1_1}, UE_{1_2} and UE_{1_3}, it is clear that the time slots serving UE_{1_3} are less than those serving UE_{1_1} and UE_{1_2}, which is consistent with the conclusions in Fig. 5(a).

To demonstrate that the proposed DW strategy ensures the fairness to all UAs, Fig. 6(a) depicts the RIS-UAV flight trajectory when the system adopts the initial trajectory scheme and the DW FP-SCA trajectory optimization scheme, respectively. Comparing it with Fig. 5(a), it is evident that the DW FP-SCA algorithm achieves a more balanced distribution of time slots for the RIS-UAV hovering above UE_{1_1}, UE_{1_2} and UE_{1_3}. Fig. 6(b) further illustrates the weighted UE rate and the corresponding sum rate under different time slots. In contrast to Fig. 5(b), the communication service time slots for UE_{1_1}, UE_{1_2} and UE_{1_3} are more evenly allocated.

Fig. 7 depicts the convergence times as the functions of the number of time slots N achieved by two algorithms, given two values of K. As expected, the convergence time increases with the increase of N. Similarly, increasing K leads to the increase of the convergence time. Notably, the FP-SCA algorithm achieves a lower convergence time compared to the traditional SCA algorithm, which is consistent with the analysis in Section 4.

Fig. 8 illustrates the system WSRs as the functions of the RIS-UAV height H for various RIS-UAV trajectory non-optimization/optimization schemes. It can be seen that increasing the RIS-UAV flight altitude reduces the system WSR for all RIS-UAV trajectory schemes. This is because an increase in the RIS-UAV height leads to a longer channel distance and higher path loss, thereby reducing the system WSR. The proposed FP-SCA algorithm outperforms the traditional SCA algorithm in terms of WSR. This superiority is due to the FP algorithm's ability to eliminate higher-order power terms and nested operations, which enhances the algorithm's optimization performance. As expected, when the RIS employs a random $\mathbf{\Phi}$, the system WSR performance drops significantly. In this scenario, the DW FP-SCA algorithm still maintains a higher WSR than the other methods.

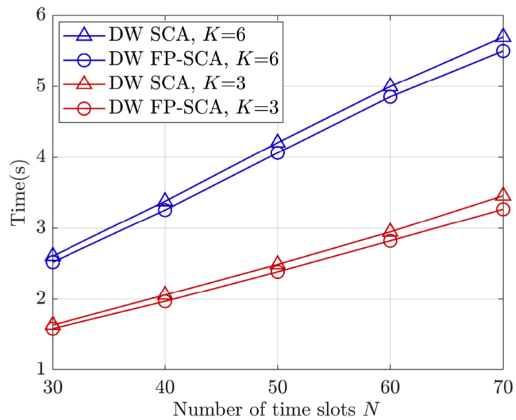

Fig. 7. Convergence times versus number of time slots N for the traditional SCA and the proposed FP-SCA given two different numbers of total UEs K.

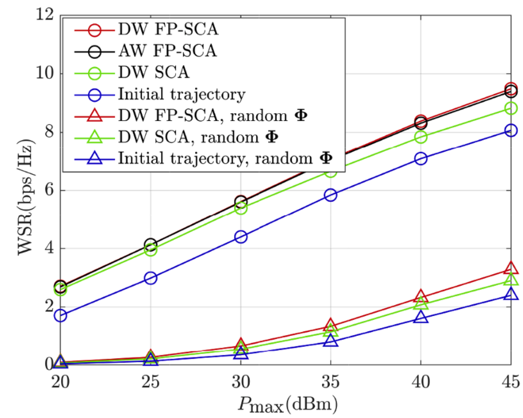

Fig. 9. WSR versus BS maximum transmit power $P_{\max}$ for various RIS-UAV trajectory non-optimization/optimization schemes.

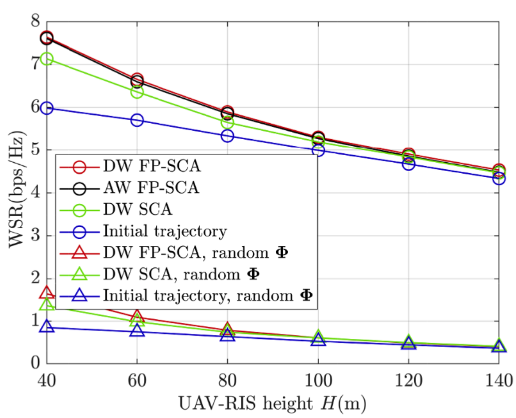

Fig. 8. WSR versus RIS-UAV height H for various RIS-UAV trajectory non-optimization/optimization schemes.

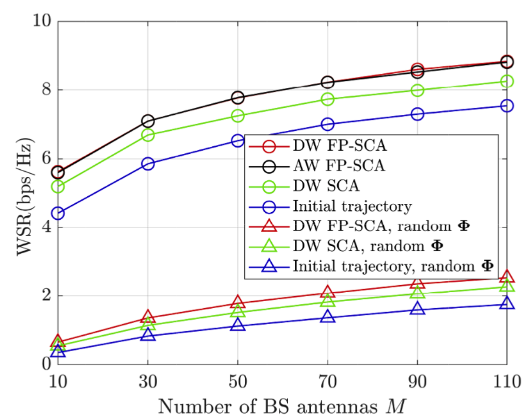

Fig. 10. WSR versus number of BS antennas M for various RIS-UAV trajectory non-optimization/optimization schemes.

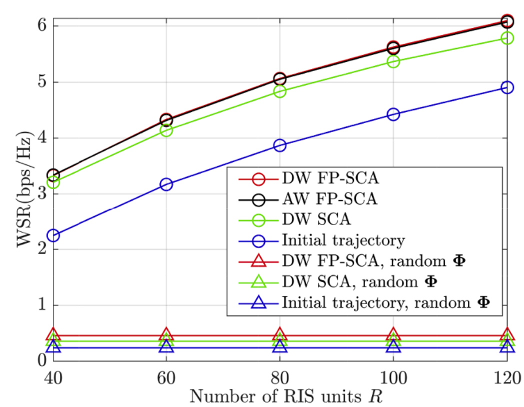

Fig. 11. WSR versus number of RIS units R for various RIS-UAV trajectory non-optimization/optimization schemes.

Fig. 9 plots the system's WSR performance as the functions of the BS maximum transmit power $P_{\max}$ for different RIS-UAV trajectory designs. Not surprisingly, the WSRs of all the RIS-UAV trajectory designs increase as the BS maximum transmit power increases. This is because the signal energy in the channel that can be harvested and utilized increases as the BS transmit power increases. Furthermore, the DW FP-SCA algorithm proposed in this paper consistently exhibits higher WSR performance than the other corresponding algorithms.

A simulation plot given in Fig. 10 shows the system WSR performance as the functions of the number of BS antennas M for various RIS-UAV trajectory designs. It can be seen that the WSRs of all the RIS-UAV trajectory designs increase with the number of BS antennas M. More antennas mean that the BS antenna array can concentrate energy more efficiently in the target direction, thereby improving the signal transmission quality. This results in a higher strength of the received signal at the same transmit power and a corresponding increase in the SINR, leading to an increasing trend in WSR for all the RIS-UAV trajectory design schemes.

The impact of the number of RIS units R on the achievable system WSR is investigated in Fig. 11. It can be observed that with the increase in the number of RIS units R, the WSRs of all the RIS-UAV trajectory design schemes, except for those with the random $\mathbf{\Phi}$, show an increasing trend. This is due to the fact that the RIS can adjust the phase and amplitude of its units by intelligently tuning them, and with the increase in the number of RIS units R, the gain of the reflected signals is significantly increased, leading to an increase in the strength of the received signals and the SINR. From Fig. 11, we observe that the proposed ARIS-UAV achieves a given WSR with fewer RIS elements R than the PRIS-UAV baseline. Since the RIS weight and power consumption scale with R, the ARIS-UAV offers a lighter payload, leading to reduced propulsion power and improved flight endurance, which are key constraints in UAV systems [7],[8].

6. Conclusion

This paper has proposed a RIS-UAV assisted MAU communication system which maximizes the system WSR by jointly optimizing the BS power allocation, the active/passive beamforming and the RIS-UAV trajectory, while ensuring the fairness of communication services for the UAs. Specifically, we have designed a PAC joint optimization algorithm framework to decompose the WSR maximization problem into two phases, which are the joint optimization phase of BS power allocation and active/passive beamforming, and the optimization phase of RIS-UAV trajectory. In the first phase, we have first simplified the problem based on the FP algorithm, and then solved it using the convex and manifold optimization algorithms. In the second phase, to ensure communication services fairness in the MAU system, we have proposed a DW FP-SCA trajectory optimization algorithm based on distance information. Simulation results demonstrate that the proposed DW-FP-SCA algorithm not only effectively ensures balanced downlink data transmission among MAU users, but also achieves significant performance gains with lower computational complexity than the traditional SCA algorithm.

CRediT authorship contribution statement

Xinying Guo: Supervision, Conceptualization; **Longfei Liu:** Writing – original draft, Formal analysis, Data curation; **Yi Song:** Methodology; **Jiankang Zhang:** Investigation; **Sheng Chen:** Writing – review & editing.

Ethics declaration

The author(s) declare(s) that the study does not involve humans nor animal subjects.

Declaration of competing interest

The authors declare that they have no known competing financial interests or personal relationships that could have appeared to influence the work reported in this paper.

Acknowledgments

This work was supported by the National Natural Science Foundation of China (Grant 61901159, 62172141).

Data availability

Data will be made available on request.

References

[1] X. Guo, P. Zhao, J. Zhang, Y. Song, S. Chen, Energy efficiency maximization for RIS-UAVs aided communication networks: a joint optimization framework, IEEE Wirel. Commun. Lett. 15 (2026) 4440–4444.
[2] B. Yang, T. Taleb, Y. Shen, X. Jiang, W. Yang, Performance, fairness, and tradeoff in UAV swarm underlaid mmWave cellular networks with directional antennas, IEEE Trans. Wirel. Commun. 20 (4) (2021) 2383–2397.
[3] R. Fan, J. Cui, S. Jin, K. Yang, J. An, Optimal node placement and resource allocation for UAV relaying network, IEEE Commun. Lett. 22 (4) (2018) 808–811.
[4] J. Gong, J. Lin, T.-H. Chang, C. Shen, X. Chen, Distributed power allocation for UAV-assisted multi-user relay networks, in: 2018 11Th International Symposium on Communication Systems, Networks & Digital Signal Processing (CSNDSP), 2018, pp. 1–6.
[5] Q. Song, F. Zheng, Energy efficient multi-antenna UAV-enabled mobile relay, China Commun. 15 (5) (2018) 41–50.
[6] Q. Chen, Joint position and resource optimization for multi-UAV-aided relaying systems, IEEE Access 8 (2020) 10403–10415.
[7] X. Jiang, M. Sheng, N. Zhao, C. Xing, L.U. Weidang, X. Wang, Green UAV communications for 6G: a survey, Chin. J. Aeronaut. 35 (9) (2022) 19–34.
[8] A. Thibbotuwawa, P. Nielsen, B. Zbigniew, G. Bocewicz, Factors affecting energy consumption of unmanned aerial vehicles: an analysis of how energy consumption changes in relation to UAV routing, in: 2018 39Th International Conference on Information Systems Architecture and Technology (ISAT), 2018, pp. 228–238.
[9] X. Pang, M. Sheng, N. Zhao, J. Tang, D. Niyato, K.-K. Wong, When UAV meets IRS: expanding air-ground networks via passive reflection, IEEE Wirel. Commun. 28 (5) (2021) 164–170.
[10] M. Munochiveyi, A.C. Pogaku, D.-T. Do, A.-T. Le, M. Voznak, N.D. Nguyen, Reconfigurable intelligent surface aided multi-user communications: state-of-the-art techniques and open issues, IEEE Access 9 (2021) 118584–118605.
[11] X. Guo, R. Yuan, J. Zhang, Y. Song, S. Chen, RSMA-Enhanced secure transmission scheme for active STAR-RIS-aided networks, IEEE Wirel. Commun. Lett. 15 (2026) 2699–2703.
[12] M. Cui, W. Han, D. Xu, P. Zhao, W. Zou, Hybrid precoding design based on alternating optimization in mmWave massive MIMO systems aided by intelligent reflecting surface, Comput. Commun. 180 (2021) 188–196.
[13] X. Li, M. Liu, S. Dang, N.C. Luong, C. Yuen, A. Nallanathan, D. Niyato, Covert communications with enhanced physical layer security in ris-assisted cooperative networks, IEEE Trans. Wirel. Commun. 24(7), 2025 5605–5619.
[14] X. Li, Z. Xie, Z. Chu, V.G. Menon, S. Mumtaz, J. Zhang, Exploiting benefits of irs in wireless powered noma networks, IEEE Trans. Green Commun. andNetworking 6(1), 2025 175–186.
[15] Z. Chen, J. Tang, X.Y. Zhang, Q. Wu, G. Chen, K.-K. Wong, Robust hybrid beamforming design for multi-RIS assisted MIMO system with imperfect CSI, IEEE Trans. Wirel. Commun. 22 (6) (2023) 3913–3926.
[16] H. Niu, Z. Chu, F. Zhou, Z. Zhu, M. Zhang, K.-K. Wong, Weighted sum secrecy rate maximization using intelligent reflecting surface, IEEE Trans. Commun. 69 (9) (2021) 6170–6184.
[17] A. Rafieifar, H. Ahmadinejad, S.M. Razavizadeh, J. He, Secure beamforming in multi-user multi-IRS millimeter wave systems, IEEE Trans. Wirel. Commun. 22 (9) (2023) 6140–6156.
[18] J. Bao, Y. Cao, J. Tang, L. Xu, N. Zhao, X. Wang, Secrecy energy efficiency enhancement of active IRS aided MISO networks, IEEE Trans. Veh. Technol. 73 (5) (2024) 7345–7350.
[19] Q. Wu, R. Zhang, Beamforming optimization for wireless network aided by intelligent reflecting surface with discrete phase shifts, IEEE Trans. Commun. 68 (3) (2020) 1838–1851.
[20] Z. Yang, M. Chen, W. Saad, W. Xu, M. Shikh-Bahaei, H.V. Poor, S. Cui, Energy-efficient wireless communications with distributed reconfigurable intelligent surfaces, IEEE Trans. Wirel. Commun. 21 (1) (2022) 665–679.
[21] M. Li, X. Tao, N. Li, H. Wu, Energy-efficient covert communication with the aid of aerial reconfigurable intelligent surface, IEEE Commun. Lett. 26 (9) (2022) 2101–2105.
[22] K. Weinberger, S. Tewes, J. Müller, R. Dyrska, M. Mönnigmann, A. Sezgin, Flying intelligent surfaces: joint adjustment of position and configuration for UAV-mounted RIS, in: 2023 IEEE 97th Vehicular Technology Conference (VTC2023-Spring), 2023, pp. 1–5.
[23] H. Long, M. Chen, Z. Yang, Z. Li, B. Wang, X. Yun, M. Shikh-Bahaei, Joint trajectory and passive beamforming design for secure UAV networks with RIS, in: 2020 IEEE Globecom Workshops (GC Wkshps), 2020, pp. 1–6.
[24] S. Li, B. Duo, X. Yuan, Y.-C. Liang, M. Di Renzo, Reconfigurable intelligent surface assisted UAV communication: joint trajectory design and passive beamforming, IEEE Wirel. Commun. Lett. 9 (5) (2020) 716–720.
[25] X. Pang, N. Zhao, J. Tang, C. Wu, D. Niyato, K.-K. Wong, IRS-assisted secure UAV transmission via joint trajectory and beamforming design, IEEE Trans. Commun. 70 (2) (2022) 1140–1152.
[26] Y. Su, X. Pang, S. Chen, X. Jiang, N. Zhao, F.R. Yu, Spectrum and energy efficiency optimization in IRS-assisted UAV networks, IEEE Trans. Commun. 70 (10) (2022) 6489–6502.
[27] C.Y. Goh, C.Y. Leow, R. Nordin, Energy efficiency of unmanned aerial vehicle with reconfigurable intelligent surfaces: a comparative study, Drones 7 (2) (98, 2023).
[28] X. Liu, Y. Yu, F. Li, T.S. Durrani, Throughput maximization for RIS-UAV relaying communications, IEEE Trans. Intell. Transp. Syst. 23 (10) (2022) 19569–19574.
[29] H. Peng, L.-C. Wang, Energy harvesting reconfigurable intelligent surface for UAV based on robust deep reinforcement learning, IEEE Trans. Wirel. Commun. 22 (10) (2023) 6826–6838.
[30] H. Nguyen-Kha, H.V. Nguyen, M.T.P. Le, O.-S. Shin, Joint UAV placement and IRS phase shift optimization in downlink networks, IEEE Access 10 (2022) 111221–111231.
[31] S. Li, H. Du, D. Zhang, K. Li, Joint UAV trajectory and beamforming designs for RIS-assisted MIMO system, IEEE Trans. Veh. Technol. 73 (4) (2024) 5378–5392.
[32] Q. Zhang, J. Zhao, R. Zhang, L. Yang, Downlink transmissions of UAV-RIS-assisted cell-free massive MIMO systems: location and trajectory optimization, Sensors 24 (13) 4064, (2024).
[33] M.-H.T. Nguyen, E. Garcia-Palacios, T. Do-Duy, O.A. Dobre, T.Q. Duong, UAV-Aided aerial reconfigurable intelligent surface communications with massive MIMO system, IEEE Trans. Cogn. Commun. Netw. 8 (4) (2022) 1828–1838.
[34] X. Li, Q. Wang, M. Zeng, Y. Liu, S. Dang, T.A. Tsiftsis, O.A. Dobre, Physicallayer authentication for ambient backscatter-aided noma symbiotic systems, IEEE Trans. Commun. 71 (4), 2023 2288–2303.
[35] X. Li, M. Zhao, M. Zeng, S. Mumtaz, V.G. Menon, Z. Ding, O.A. Dobre, Hardware impaired ambient backscatter noma systems: reliability and security, IEEE Trans. Commun. 69 (4), 2021 2723–2736.
[36] S. Lv, X. Xu, S. Han, P. Zhang, UAV-RIS-Assisted coordinated multipoint finite blocklength transmission for MTC networks, IEEE Internet Things J. 10 (23) (2023) 20323–20341.
[37] X. Guo, L. Liu, J. Zhang, S. Chen, Joint optimization of power allocation and beamforming for UAV-RIS communication system, IEEE Wirel. Commun. Lett. 14 (6) (2025) 1733–1737.
[38] H. Guo, Y.-C. Liang, J. Chen, E.G. Larsson, Weighted sum-rate maximization for reconfigurable intelligent surface aided wireless networks, IEEE Trans. Wirel. Commun. 19 (5) (2020) 3064–3076.
[39] Y. Cao, T. Lv, W. Ni, Intelligent reflecting surface aided multi-user mmWave communications for coverage enhancement, in: 2020 IEEE 31st Annual International Symposium on Personal, Indoor and Mobile Radio Communications, 2020, pp. 1–6.

[40] Y. Xiu, Y. Zhao, Y. Liu, J. Zhao, O. Yagan, N. Wei, IRS-Assisted millimeter wave communications: joint power allocation and beamforming design, in: 2021 IEEE Wireless Communications and Networking Conference Workshops (WCNCW), 2021, pp. 1–6.
[41] D. Wang, Y. Zhao, Y. He, X. Tang, L. Li, R. Zhang, D. Zhai, Passive beamforming and trajectory optimization for reconfigurable intelligent surface-assisted UAV secure communication, Remote Sens. 13 (21) 4286, (2021).
[42] L. Ge, H. Zhang, J.-B. Wang, G.Y. Li, Reconfigurable wireless relaying with multi-UAV-carried intelligent reflecting surfaces, IEEE Trans. Veh. Technol. 72 (4) (2023) 4932–4947.
[43] Y. Yu, X. Liu, Z. Liu, T.S. Durrani, Joint trajectory and resource optimization for RIS assisted UAV cognitive radio, IEEE Trans. Veh. Technol. 72 (10) (2023) 13643–13648.
[44] S. Li, C. Liu, H. Lei, N. Wang, X. Guo, Joint channel estimation and blockage diagnosis in RIS-assisted mmWave MIMO-OFDM systems, IEEE Trans. Veh. Technol. 75 (5) (2026) 8018–8029.
[45] S. Li, H. Lei, Z. Dong, R. Yang, X. Guo, Two-stage channel estimation in mmWave MIMO systems with RIS blockage, IEEE Wirel. Commun. Lett. 13 (12) (2024) 3548–3552.